International Symposium
On Turbulence and Shear Flow
Phenomena (TSFP-9)
June 30 - July 3, 2015 *Melbourne, Australia*

DIRECT NUMERICAL SIMULATION OF SURFACE TENSION EFFECTS ON INTERFACE DYNAMICS AND ENERGY TRANSFER IN TURBULENCE

Jeremy McCaslin
Sibley School of Mechanical and Aerospace Engineering
Cornell University
245 Upson Hall, Ithaca, NY 14853 USA
jom48@cornell.edu

Olivier Desjardins
Sibley School of Mechanical and Aerospace Engineering
Cornell University
250 Upson Hall, Ithaca, NY 14853 USA
olivier.desjardins@cornell.edu

ABSTRACT

The interaction between turbulence and surface tension is studied through direct numerical simulation of a canonical multiphase flow. An initially flat interface is inserted into a triply periodic box of decaying homogeneous isotropic turbulence, simulated for a variety of turbulent Reynolds and Weber numbers on mesh sizes of 512^3 and 1024^3. Unity density and viscosity ratios are used in order to isolate the interaction between fluid inertia and the surface tension force. Interface height correlations and liquid volume fraction variance spectra are used to study the spatial scales of corrugations on the interface. A case with zero surface tension is first considered, yielding a passive interface that moves materially with the fluid. The power spectral density of the liquid volume fraction variance follows a κ^{-1} scaling, where κ is the wavenumber, which is consistent with dimensionality arguments. In the presence of surface tension, this corrugation spectrum follows a κ^{-1} scaling for large scales, but then deviates at a length scale wich corresponds to the critical radius. A spectral analysis of liquid volume fraction variance transfer is conducted, shedding light on the role played by surface tension in this process. Results will be used to deduce important ramifications for sub-grid scale models in large-eddy simulations of liquid-gas flows.

INTRODUCTION

Interactions between turbulence and immiscible interfaces are ubiquitous in both natural environments and engineering applications, such as the dynamics of the upper ocean and primary liquid atomization in combustion devices. Liquid fueled combustion is accomplished through a variety of ways, such as pressure injection in Diesel engines or coaxial air-blast injectors in aircraft engines. A detailed description of primary atomization has remained elusive, due in part to insufficient understanding of how topologically complex interfaces modulate their surrounding flow fields. Primary air-blast atomization has been understood in recent years as a mechanistic progression of linear instabilities that destabilize the liquid core (Raynal *et al.*, 1997; Marmottant & Villermaux, 2004; Rayana *et al.*, 2006). However, while useful in certain canonical flows, in particular in mostly parallel and laminar flows, this sort of approach is less useful for describing atomizing liquids in complex geometries or in the presence of turbulence. The assumptions of linear stability analysis break down in presence of a significant non-zero normal velocity at the interface. Full characterization and subsequent modeling of liquid-gas turbulent flows in such complex scenarios requires a more general theory of turbulent atomization. Though numerical studies in this direction are limited, some progress has been made. Turbulence-interface interactions have been studied in two-dimensional simulations via an interfacial particle-level set method Li & Jaberi (2009), highlighting the interplay between surface tension and baroclinity near the interface, either of which can enhance turbulent kinetic energy (TKE) dissipation in this region. Trontin *et al.* (2010) isolate the interaction between fluid inertia and surface tension by simulating a slab of fluid in a box of three-dimensional decaying homogeneous isotropic turbulence (HIT) with unity density and viscosity ratios, examining anisotropic effects of surface tension on surrounding turbulence. A general theory of turbulent atomization must encompass these types of effects, as well as other physical processes by which a phase interface modulates a surrounding turbulent flow field.

The goal of the present study is to further the development of turbulent atomization theory by studying numerical simulations of canonical liquid-gas turbulent configurations, isolating different physical mechanisms present in the atomization process. As a starting point, we isolate the interplay between a turbulent fluid and surface tension by inserting an interface into a box of homogeneous isotropic turbulence. Short-time deformation of an initially flat interface in a field of decaying homogeneous isotropic tur-

bulence (HIT) is studied in effort to develop a statistical description of how surface tension impacts the resulting corrugations that form on the interface. Results show that interfacial corrugations follow classical turbulent scalings up to a surface tension-defined length scale, after which interface statistics are controlled by surface tension. The surface tension length scale extracted from the simulations agrees very well with the critical radius (Kolmogorov, 1949; Hinze, 1955).

DIRECT NUMERICAL SIMULATIONS

The equation for the velocity fluctuation $\mathbf{u}'$ simulated herein is written as

$$\frac{\partial \mathbf{u}'}{\partial t} + \mathbf{u}' \cdot \nabla \mathbf{u}' = -\frac{\nabla p}{\rho} + \nu \nabla^2 \mathbf{u}' + A\mathbf{u}' + \frac{\sigma}{\rho}\gamma\delta(\mathbf{x}-\mathbf{x}_\Gamma)\mathbf{n}, \quad (1)$$

where p is the pressure, ρ is the density, ν is the kinematic viscosity, γ is the curvature of the interface, δ is the Dirac delta function, $\mathbf{x}_\Gamma$ is the point on the interface Γ closest to $\mathbf{x}$, $\mathbf{n}$ is the unit vector normal to Γ, and the forcing term $A\mathbf{u}'$ acts as a source term of turbulent kinetic energy. The inclusion of the last term in Eq. (1) accounts for the singular surface tension force at the interface. The forcing coefficient $A = 1/3\tau$ was introduced by Lundgren (2003) and dictates the large-eddy turnover time of the flow field, τ. Rosales & Meneveau (2005) have shown that this linear forcing methodology yields turbulence statistics that are nearly indistinguishable from band-limited forcing in spectral space.

Generation of homogeneous isotropic turbulence

To generate a field of statistically stationary homogeneous isotropic turbulence (HIT), Eq. (1) is first evolved with $\sigma = 0$ within the NGA code (Desjardins *et al.*, 2008) in a triply periodic box of size $(2\pi)^3$. The resulting Taylor-microscale Reynolds number $\mathrm{Re}_\lambda = u_{\mathrm{rms}}\lambda_g/\nu$ is based on the root-mean-square velocity u_{rms} and the Taylor microscale $\lambda_g = \sqrt{10}(\eta^2\mathscr{L})^{1/3}$, where η is the Kolmogorov length scale and $\mathscr{L}$ is the characteristic length scale of the large eddies. This length scale $\mathscr{L} = k^{3/2}/\varepsilon$ is defined in terms of the TKE k, written as $k = 3u_{\mathrm{rms}}^2/2$, and ε, which is the dissipation rate of TKE. All values of Re_λ considered in the present study exhibit a classical $-5/3$ inertial subrange.

Turbulent interfacial flow

Once the HIT becomes statistically stationary, the forcing coefficient A in Eq. (1) is set to zero and the HIT decays with an interface distribution that is initially flat. Because ρ and ν are uniform everywhere, the only discontinuity is in the pressure field, and we write the jump in pressure $[p]_\Gamma$ as $[p]_\Gamma = \sigma\gamma$. The ghost fluid method (Fedkiw *et al.*, 1999) is used to handle the pressure jump across the interface, and details regarding the implementation of Eq. (1) (for the more general case of variable density) are provided by Desjardins *et al.* (2008).

The recent volume-of-fluid (VOF) method of Owkes & Desjardins (2014) is coupled to NGA (Desjardins *et al.*, 2008) in order to capture the interface. The semi-Lagrangian, flux-based VOF scheme provides discrete consistency between mass and momentum transport through geometric calculation of flux volumes. The resultant scheme provides second order accuracy in space and time, exact conservation of mass and momentum everywhere in the domain, conservation of kinetic energy away from the interface, and is combined with a second order curvature calculation.

Uniform density and viscosity ratios utilized herein isolate the interplay between the inertial content of the turbulent fluid and the surface tension of the interface. We have run with different values of σ, leading to a range of turbulent Weber numbers, defined as $\mathrm{We}_\lambda = \rho u_{\mathrm{rms}}^2\lambda_g/\sigma$. Table 1 summarizes the simulations.

Table 1. Parameters that characterize the HIT/interface simulations.

Case	Mesh	Re_λ	We_λ
0	1024^3	313	∞
1	1024^3	313	8.47
2	1024^3	313	1.36
3	1024^3	313	0.22
4	512^3	194	8.47
5	512^3	194	1.36
6	512^3	194	0.22

THE IMPACT OF SURFACE TENSION ON THE INTERFACE

The four cases shown in Fig. 1 are Case 0 – 3. Case 0 corresponds to $\mathrm{We}_\lambda = \infty$ ($\sigma = 0$), for which the interface moves materially with the fluid. It is observed from Fig. 1 that the large-scale variations of the interface are similar for each case, while small scale interfacial corrugations become increasingly suppressed as We_λ decreases. The same observation can be made for cases with $\mathrm{Re}_\lambda = 194$.

The spectral footprint of surface tension

The interfacial feature suppression by surface tension that is evident in Fig. 1 is quantified by defining $\alpha(\mathbf{x})$ as the volume fraction of fluid 1, i.e., the fluid beneath the initially flat interface. The volume fraction fluctuation α' is computed as $\alpha'(\mathbf{x}) = \alpha(\mathbf{x}) - \langle\alpha(\mathbf{x})\rangle_{x,z}$, where $\langle * \rangle_{x,z}$ denotes an average with respect to coordinates x and z. Denoting y as the direction normal to the initially flat interface, we compute the auto-covariance of $\alpha'(x, y = 0, z)$ (i.e., at the location of the initially flat interface) as $R_\alpha(r_x, r_z) = \langle\alpha'(x,0,z)\,\alpha'(x+r_x,0,z+r_z)\rangle_{x,z}$. Taking the Fourier transform of R_α gives the liquid volume fraction variance spectrum $\widehat{R}_\alpha$, written as

$$\widehat{R}_\alpha(\kappa_x,\kappa_z) = \frac{1}{2\pi}\int\int R_\alpha(r_x,r_z)e^{-i(\kappa_x r_x+\kappa_z r_z)}\,\mathrm{d}r_x\mathrm{d}r_z, \quad (2)$$

where κ_x and κ_z are the wavenumbers in x and z, respectively. Figure 2(a) shows plots of the compensated spectrum $\kappa\widehat{R}_\alpha(\kappa)$ for cases 0 – 3 plotted as a function of $\kappa\eta$, where

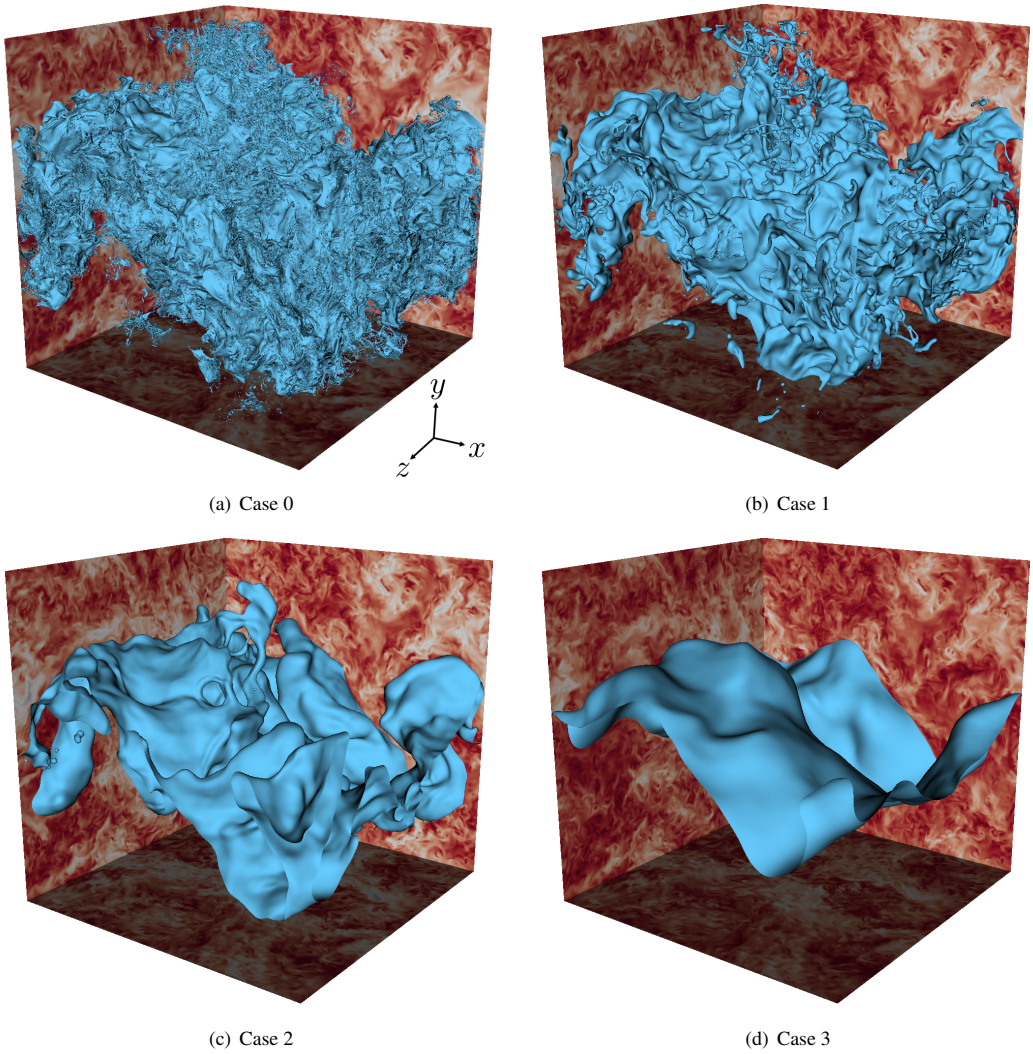

(a) Case 0 (b) Case 1

(c) Case 2 (d) Case 3

Figure 1. Topology of the interface after half a large-eddy turnover time. Color indicates velocity magnitude of the surrounding turbulent flow, ranging from 0 (red) to maximum value (white).

$\kappa = (\kappa_x^2 + \kappa_y^2)^{1/2}$ and η is the Kolmogorov scale of the initial turbulent flow field. Note that the result looks the same for cases 4 – 6 (at a lower Re_λ), so only the high Re_λ results are shown for clarity. For case 0 in which the interface moves materially with the fluid (no surface tension), $\kappa\widehat{R}_\alpha$ is quite flat for roughly two decades before transport due to low mesh resolution affects the spectrum. This is due to the fact that even in the absence of physical surface tension, our VOF transport scheme at low mesh resolution introduces a numerical surface tension. This flat region means that $\widehat{R}_\alpha \sim \kappa^{-1}$, which is consistent with the findings of Lesieur & Rogallo (1989), who reported a range of κ^{-1} scaling for the variance of passive scalars in turbulence, followed by $\kappa^{-5/3}$ scaling. The extent to which the passive temperature field of Lesieur & Rogallo (1989) experiences a κ^{-1} depends on the relative decay of temperature variance versus kinetic energy. In the case of α with $\sigma = 0$, however, there is no analog to diffusion, and $\widehat{R}_\alpha \sim \kappa^{-1}$ for all resolved scales.

The spectra for cases 1 and 2 also show a κ^{-1} region, but the presence of surface tension is evident through the distinct change in scaling once a limiting wavenumber κ_σ is reached. Once $\kappa \approx \kappa_\sigma$, $\widehat{R}_\alpha$ assumes a κ^{-2} scaling, as evidenced by the clear κ^{-1} of the compensated spectra for $\kappa > \kappa_\sigma$. In case 3, surface tension is so large that surface corrugations are suppressed on even the largest scales, and $\widehat{R}_\alpha \sim \kappa^{-2}$ for all scales. Note that we also observe the same two-slope type of behavior in wave spectra (defined similarly to the wave spectra of Phillips 1977) and surface density variance spectra.

We observe that the critical wavenumber κ_σ is predicted very well by $\kappa_\sigma = 2\pi/l_\sigma$, where

$$l_\sigma \sim \left(\frac{\sigma^3}{\rho^3\varepsilon^2}\right)^{1/5} \tag{3}$$

is the critical length scale below which interfacial corrugations are suppressed by surface tension (Kolmogorov, 1949; Hinze, 1955). The critical length scale l_σ is extracted for all simulations in Table 1 and compared to the predicted value from Eq. (3), and good agreement is observed in Fig. 2(b).

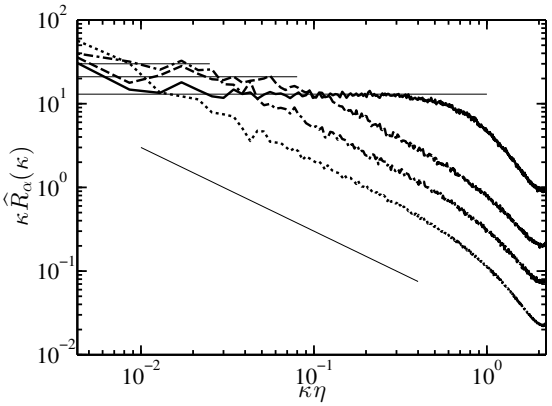

(a) $\kappa\widehat{R}_\alpha$ for the $\mathrm{Re}_\lambda = 313$ cases. Case 0 (thick solid); case 1 (dashed); case 2 (dash-dotted); case 3 (dotted). Thin horizontal lines highlight regions $\sim \kappa^0$; the thin diagonal line shows κ^{-1} for comparison.

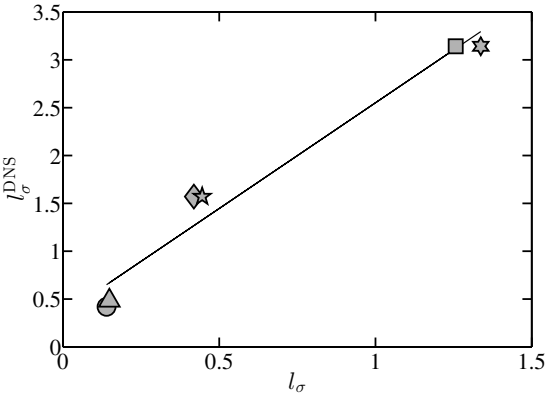

(b) Predicted l_σ compared to measured l_σ^{DNS}: case 1 (circle); case 2 (diamond); case 3 (square); case 4 (triangle); case 5 (pentagram); case 6 (hexagram); best fit (line).

Figure 2. Liquid volume fraction variance spectra for Cases 0 – 3 and comparison between predicted and measured l_σ.

Interface curvature statistics

Surface tension suppresses interface corrugations and therefore acts to prevent regions of high curvature. The probability density function (PDF) of maximum curvature $\gamma_{\max}$ is shown in Fig. 3(a) for cases 0 – 6, defined as $\gamma_{\max} = \max(|\gamma_1|, |\gamma_2|)$, where γ_1 and γ_2 are the two principal curvatures. PDFs were also computed for the curvedness, defined as $\sqrt{(\gamma_1^2+\gamma_2^2)/2}$ (Koenderink & van Doorn, 1992), but the difference was negligible.

The peak for each PDF in Fig. 3(a) shifts to the left as We_λ decreases, due to the prevention of high curvatures by surface tension. The curvature distribution decreases beyond the peak value rapidly for the lowest Weber number, which is in qualitative agreement with the relatively flat interface in Fig. 1(d). Curvatures approaching $1/\Delta x$ (where Δx is the mesh spacing) are orders of magnitude more probable for case 0 than for all cases with surface tension, as no physical mechanism prevents interfacial features on the scale of the mesh size to develop. The PDFs look similar for each pair of cases with the same We_λ, indicating that the principal curvature distribution is not a strong function of Re_λ.

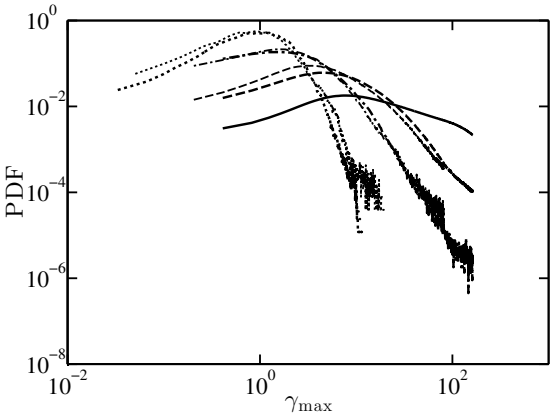

(a) Unnormalized curvature $\gamma_{\max}$

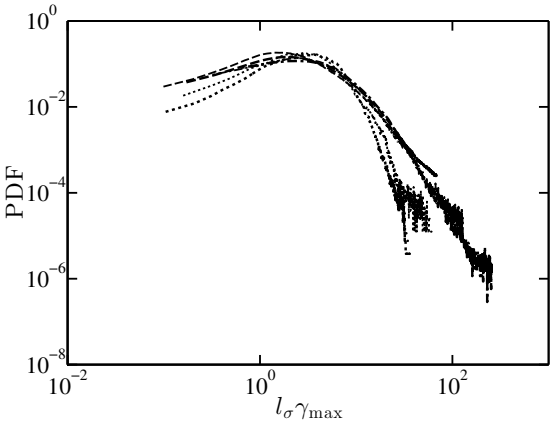

(b) Normalized curvature $l_\sigma\gamma_{\max}$

Figure 3. PDFs of maximum principal curvature: case 0 (solid); case 1 (thick dashed); case 2 (thick dash-dotted); case 3 (thick dotted); case 4 (thin dashed); case 5 (thin dash-dotted); case 6 (thin dotted).

Interestingly, the PDFs for all cases show reasonable collapse on one another when normalizing $\gamma_{\max}$ by the critical length scale, as seen in the PDFs of $l_\sigma\gamma_{\max}$ in Fig. 3(b). Cases 3 and 6 with the lowest We_λ peak near $l_\sigma\gamma_{\max} \approx 3$, while cases 1, 2, 4, and 5 peak near $l_\sigma\gamma_{\max} \approx 2$. The collapse of the peak values of $\gamma_{\max}$ near l_σ supports the idea that turbulence corrugates the interface by wrinkling and folding it to smaller and smaller scales, creating larger and larger curvatures, until the critical length scale is reached, and surface tension acts against further wrinkling and folding.

Liquid volume fraction variance transfer

We study the effect that surface tension has on the transfer of liquid volume fraction variance by decomposing the α field as $\alpha = \widetilde{\alpha} + \alpha'$, where $\widetilde{\alpha}$ is the result of filtering α on a scale Δ and α' is the sub-filter part of α. This allows us to study the filtered quantity part as a function of the filter size Δ. The filtered quantity $\widetilde{\alpha}$ is obtained by taking the convolution of α with the kernel g:

$$\widetilde{\alpha}(\mathbf{x}) = \frac{1}{\mathscr{V}} \int_{\mathscr{V}} \alpha(\mathbf{x}')\, g\left(|\mathbf{x}-\mathbf{x}'|\right) \mathrm{d}\mathbf{x}'. \qquad (4)$$

We write the α transport equation as

$$\frac{\partial \alpha}{\partial t} + \nabla \cdot (\mathbf{u}\alpha) = 0\,, \tag{5}$$

where $\mathbf{u}\cdot\nabla\alpha = \nabla\cdot(\mathbf{u}\alpha)$ has been used due to $\nabla\cdot\mathbf{u} = 0$ (i.e., solenoidal velocity field). Applying the filter in Eq. (4) to this equation and different forms of it leads to

$$\frac{\partial \widetilde{\alpha}^2}{\partial t} + \nabla\cdot\left(\widetilde{\mathbf{u}}\widetilde{\alpha}^2\right) = -\nabla\cdot(2\widetilde{\alpha}\mathbf{R}_\alpha) - T_\alpha \tag{6}$$

$$\frac{\partial \widetilde{\alpha'^2}}{\partial t} + \nabla\cdot\left(\widetilde{\mathbf{u}}\widetilde{\alpha'^2}\right) = \nabla\cdot(2\widetilde{\alpha}\mathbf{R}_\alpha - \mathbf{R}_{\alpha 2}) + T_\alpha \tag{7}$$

$$\mathbf{R}_\alpha = \widetilde{\mathbf{u}\alpha} - \widetilde{\mathbf{u}}\widetilde{\alpha}$$

$$\mathbf{R}_{\alpha 2} = \widetilde{\mathbf{u}\alpha^2} - \widetilde{\mathbf{u}}\widetilde{\alpha^2}$$

$$T_\alpha = -2\mathbf{R}_\alpha\cdot\nabla\widetilde{\alpha}\,,$$

where Eq. (6) governs the resolved variance $\widetilde{\alpha}^2$ and Eq. (7) governs the sub-filter variance $\widetilde{\alpha'^2} = \widetilde{\alpha^2} - \widetilde{\alpha}^2$.

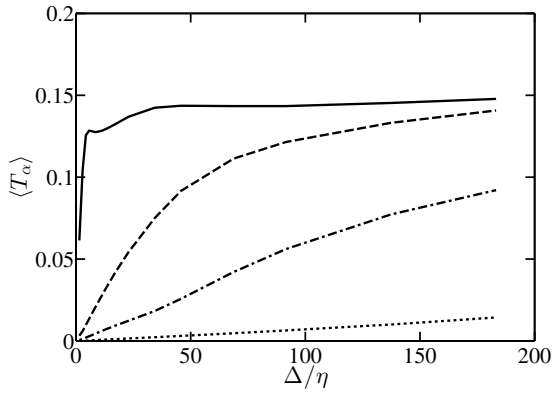

(a) Filter size Δ normalized by η

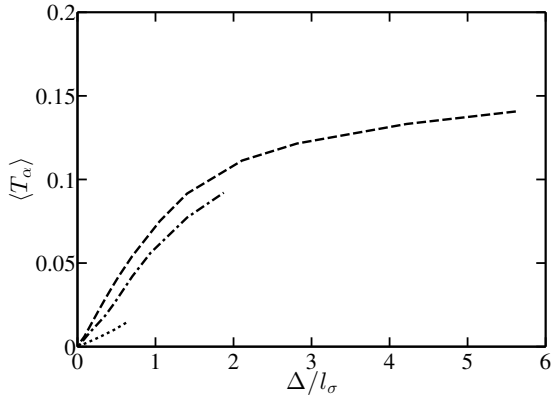

(b) Filter size Δ normalized by l_σ

Figure 4. $\langle T_\alpha \rangle$ for the $\mathrm{Re}_\lambda = 313$ cases. Case 0 (solid line); case 1 (dashed line); case 2 (dash-dotted line); case 3 (dotted line).

Inspecting Eqs. (6) and (7), we see that first term on the RHS of each equation is a conservative diffusion term. The last term T_α, which appears with opposite sign in each equation, is non-conservative and represents the transfer rate of α variance from the resolved to sub-filter scales. Figure 4(a) shows the globally averaged $\langle T_\alpha \rangle$ for each $\mathrm{Re}_\lambda = 313$ case. For case 0 with $\sigma = 0$, $\langle T_\alpha \rangle$ is constant and goes to zero for $\Delta \approx \eta$, indicating that the transfer decay is controlled by lack of mesh resolution at the Kolmogorov scale. For cases 1 – 3, however, it is clear that η does not control the onset of $\langle T_\alpha \rangle$ decay. Figure 4(b) shows that $\langle T_\alpha \rangle$ begins to decay near a value of $\Delta/l_\sigma \approx 1$, indicating that transfer of α variance is suppressed near the critical length scale. Note that this trend cannot be observed for case 3, because $l_\sigma \sim L$ and there is no well-defined large length scale that is sufficiently larger than l_σ.

Backscatter of α variance by surface tension

The role played by surface tension in the α variance and kinetic energy transfer process can be further understood by examining the transfer terms that arise from a model velocity field induced purely by surface tension. Noting that the instantaneous acceleration of fluid due to surface tension can be written as $\mathbf{a}_\sigma = \sigma\gamma\nabla\alpha$, we can write such a model velocity as

$$\mathbf{u}^{\mathrm{mod}} = \int_{t_0}^{t_0+\Delta t} \mathbf{a}_\sigma \,\mathrm{d}t' \approx \sigma\gamma\nabla\alpha\,\Delta t\,, \tag{8}$$

where $\mathbf{u}^{\mathrm{mod}}(t_0) = 0$ and Δt is small such that the change in γ and $\nabla\alpha$ over Δt is negligible. The mean α variance

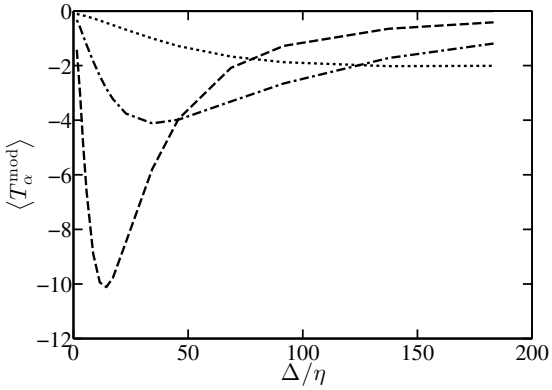

Figure 5. α variance transfer term computed from $\mathbf{u}^{\mathrm{mod}}$ for $\mathrm{Re}_\lambda = 313$ cases: case 0 (solid line); case 1 (dashed line); case 2 (dash-dotted line); case 3 (dotted line).

transfer term $\langle T_\alpha^{\mathrm{mod}} \rangle$ is computed from $\mathbf{u}^{\mathrm{mod}}$ for cases with $\mathrm{Re}_\lambda = 313$ and shown in Fig. 5 (normalized by Δt, which is taken to be the simulation time step). Negative values indicate a backscatter of α variance, i.e., a transfer from sub-filter to resolved scales. Plotting the transfer as a function of Δ/l_σ shows that the backscatter is maximum near the critical length scale, as shown in figure 6(a). The α variance term has units of $(\mathrm{time})^{-1}$, and a collapse of the data is observed when $\langle T_\alpha^{\mathrm{mod}} \rangle$ is made dimensionless by the surface tension time scale $\tau_\sigma = (l_\sigma^3/\sigma)^{1/2}$, as shown in figure 6(b).

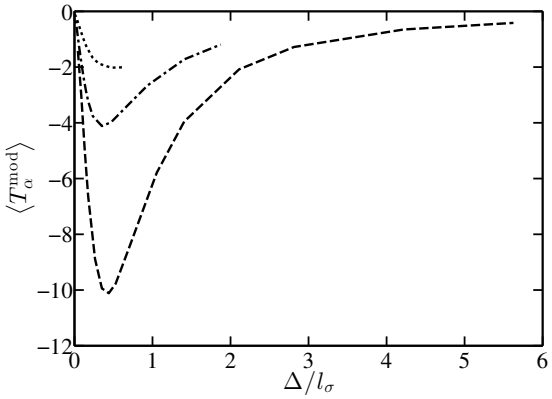

(a) Filter size Δ normalized by l_σ

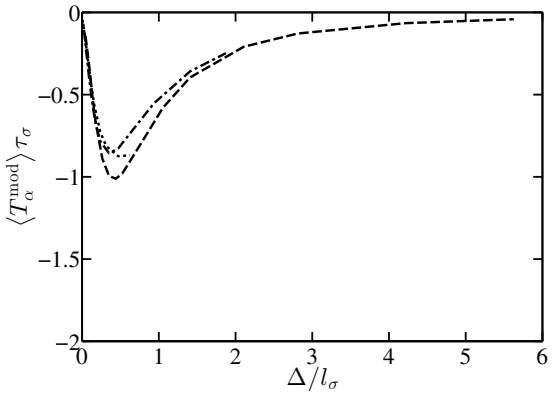

(b) Collapse of curves when normalized by time scale $\tau_\sigma = \sqrt{l_\sigma^3/\sigma}$

Figure 6. α variance transfer term computed from $\mathbf{u}^{\mathrm{mod}}$ for $\mathrm{Re}_\lambda = 313$ cases: case 1 (dashed line); case 2 (dash-dotted line); case 3 (dotted line).

CONCLUSION AND FUTURE DIRECTION

We have constructed a canonical multiphase turbulence test case that allows us to isolate the interplay between surface tension and fluid inertia. This approach allows us to statistically examine the effects of surface tension on the corrugations that form on the interface. Through spectra of liquid volume fraction fluctuations and integrated interface heights, it is observed that interface corrugations are greatly suppressed on length scales smaller than the critical radius (Kolmogorov, 1949; Hinze, 1955).

Probability density functions of principal curvature are shown over a parameter space of Reynolds number and Weber number. All curves exhibit a peak value at the critical radius, demonstrating the robustness of this length scale as a delineation between interface corrugations generated by turbulence and those suppressed by surface tension. The role of surface tension in the cascade of liquid volume fraction variance is explored through a filtering approach, highlighting the importance of the critical length scale as a source of backscatter. Work currently in development includes conducting a similar filtering approach for the fluid momentum, revealing an analogous source of backscatter for kinetic energy from sub-filter to resolved scales. Future work will include *a priori* testing of sub-grid scale models for the advancement of enhanced large-eddy simulations of liquid-gas turbulent flows.

REFERENCES

Desjardins, Olivier, Blanquart, Guillaume, Balarac, Guillaume & Pitsch, Heinz 2008 High order conservative finite difference scheme for variable density low Mach number turbulent flows. *Journal of Computational Physics* **227** (15), 7125–7159.

Fedkiw, Ronald P., Aslam, Tariq D., Merriman, Barry & Osher, Stanley 1999 A non-oscillatory Eulerian approach to interfaces in multimaterial flows (the Ghost Fluid Method). *Journal of Computational Physics* **152** (2), 457–492.

Hinze, J 1955 Fundamentals of the hydrodynamic mechanism of splitting in dispersion processes. *AIChE Journal* **1** (3), 289–295.

Koenderink, Jan J & van Doorn, Andrea J 1992 Surface shape and curvature scales. *Image and Vision Computing* **10** (8), 557–564.

Kolmogorov, AN 1949 On the breakage of drops in a turbulent flow. *Doklady Akademii Nauk SSSR* **66**, 825–828.

Lesieur, Marcel & Rogallo, Robert 1989 Large-eddy simulation of passive scalar diffusion in isotropic turbulence. *Physics of Fluids A: Fluid Dynamics* **1** (4), 718.

Li, Zhaorui & Jaberi, Farhad a. 2009 Turbulence-interface interactions in a two-fluid homogeneous flow. *Physics of Fluids* **21** (9), 095102.

Lundgren, T. S. 2003 Linearly forced isotropic turbulence. *Center for Turbulence Research Annual Research Briefs* pp. 461–473.

Marmottant, P & Villermaux, Emmanuel 2004 On spray formation. *Journal of Fluid Mechanics* **498**, 73–111.

Owkes, Mark & Desjardins, Olivier 2014 A computational framework for conservative, three-dimensional, un-split, geometric transport with application to the volume-of-fluid (VOF) method. *Journal of Computational Physics* **270**, 587–612.

Phillips, O. M. 1977 *The dynamics of the upper ocean*. Cambridge University Press.

Rayana, Fares Ben, Cartellier, Alain & Hopfinger, Emil 2006 Assisted atomization of a liquid layer: investigation of the parameters affecting the mean drop size prediction. In *Proceedings of the international conference on Liquid Atomization and Spray Systems (ICLASS)*, pp. 1–8. Kyoto, Japan.

Raynal, L, Villermaux, E, Lasheras, JC & Hopfinger, EJ 1997 Primary instability in liquid-gas shear layers. *11th Symposium on Turbulent Shear Flows* **3**, 27.1–27.5.

Rosales, Carlos & Meneveau, Charles 2005 Linear forcing in numerical simulations of isotropic turbulence: Physical space implementations and convergence properties. *Physics of Fluids* **17** (9), 095106.

Trontin, P., Vincent, S., Estivalezes, J.L. & Caltagirone, J.P. 2010 Direct numerical simulation of a freely decaying turbulent interfacial flow. *International Journal of Multiphase Flow* **36** (11-12), 891–907.